Environmental Science & Technology

Article

pubs.acs.org/est

High-Resolution Air Pollution Mapping with Google Street View Cars: Exploiting Big Data

Joshua S. Apte,*[,†] Kyle P. Messier,[†,‡] Shahzad Gani,[†] Michael Brauer,[§] Thomas W. Kirchstetter,[∥] Melissa M. Lunden,[⊥] Julian D. Marshall,[#] Christopher J. Portier,[‡] Roel C.H. Vermeulen,[▽] and Steven P. Hamburg[‡]

[†]Department of Civil, Architectural and Environmental Engineering, University of Texas at Austin, Austin, Texas 78712 United States

[‡]Environmental Defense Fund, New York, New York 10010 United States

[§]School of Population and Public Health, University of British Columbia, Vancouver V6T 1Z3 Canada

[∥]Energy Technologies Area, Lawrence Berkeley National Laboratory, Berkeley, California 94720 United States

[⊥]Aclima, Inc., 10 Lombard St., San Francisco, California 94111 United States

[#]Department of Civil and Environmental Engineering, University of Washington, Seattle, Washington 98195 United States

[▽]Institute for Risk Assessment Science, Utrecht University, Utrecht 3584 CM Netherlands

Supporting Information

ABSTRACT: Air pollution affects billions of people worldwide, yet ambient pollution measurements are limited for much of the world. Urban air pollution concentrations vary sharply over short distances (≪1 km) owing to unevenly distributed emission sources, dilution, and physicochemical transformations. Accordingly, even where present, conventional fixed-site pollution monitoring methods lack the spatial resolution needed to characterize heterogeneous human exposures and localized pollution hotspots. Here, we demonstrate a measurement approach to reveal urban air pollution patterns at 4−5 orders of magnitude greater spatial precision than possible with current central-site ambient monitoring. We equipped Google Street View vehicles with a fast-response pollution measurement platform and repeatedly sampled every street in a 30-km^2 area of Oakland, CA, developing the largest urban air quality data set of its type. Resulting maps of annual daytime NO, NO_2, and black carbon at 30 m-scale reveal stable, persistent pollution patterns with surprisingly sharp small-scale variability attributable to local sources, up to 5−8× within individual city blocks. Since local variation in air quality profoundly impacts public health and environmental equity, our results have important implications for how air pollution is measured and managed. If validated elsewhere, this readily scalable measurement approach could address major air quality data gaps worldwide.

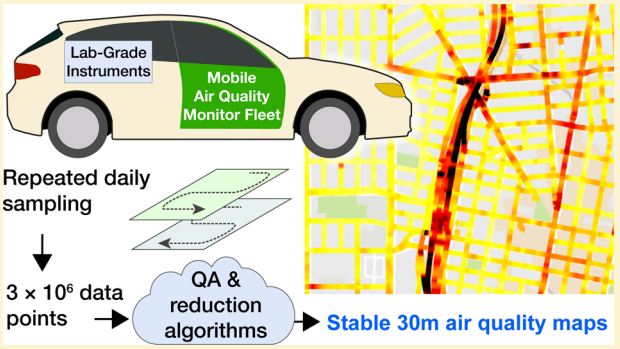

1. INTRODUCTION

Air pollution is a major global risk factor for ill-health and death.[1−4] Air pollution measurements are crucial for epidemiology and air quality management, but the extent of ground-based air pollution observations is limited.[5,6] For many developing-country regions, especially in populous parts of Asia and Africa, robust air quality monitoring is largely absent.[5] Even for high-income regions, ambient monitors are generally sparsely sited. For the 60% of the U.S. census urban areas with continuous regulatory monitoring, there are a mean of ∼2−5 monitors per million people and 1000 km^2 (Supporting Information (SI) Table S1). However, primary air pollutant concentrations in cities can vary sharply over short distances (∼0.01−1 km) owing to unevenly distributed emissions sources, dilution, and physicochemical transformations.[7−10] Such gradients are not well represented with routine ambient measurements, but have important implications for exposure assessment, epidemiology, air quality management, and environmental equity.[10−13]

Advances in air pollution exposure assessment techniques over the past two decades have helped address limitations of (i) data coverage and (ii) spatial resolution that are associated with central-site ambient monitoring.[10,14] These methods include satellite remote sensing (RS), chemical transport models (CTMs), land-use regression (LUR) models, and direct personal exposure measurements.[14] Each of these approaches has distinct advantages and limitations. Satellite RS instruments and CTMs

Received: February 17, 2017
Revised: April 26, 2017
Accepted: May 4, 2017
Published: June 5, 2017

DOI: 10.1021/acs.est.7b00891
Environ. Sci. Technol. 2017, 51, 6999−7008

are spatially coarse (>1−10 km resolution), and cannot characterize the fine-scale gradients (10−300 m) that drive population exposure to local emissions such as traffic. Satellites are unable to measure some pollutants of key health concern (e.g., black carbon, ultrafine particles). Dispersion models and CTMs are only as reliable as their underlying emissions inventories, and thus cannot reveal unexpected sources. Empirical and geostatistical models such as LUR and kriging can estimate concentrations at high spatial resolution.[10,14−17] However, these models provide limited temporal information, often require local training data sets to be available or collected, and struggle to predict the tails of air pollution distributions, especially where idiosyncratic local sources exist. Alternative methods to measure how air pollution concentrations vary *within* cities and neighborhoods could complement these existing techniques and fill important data gaps.[18,19]

We explore here the potential of routine mobile monitoring with fleet vehicles for measuring time-integrated concentrations at high spatial resolution. The use of vehicles for mobile air pollution sampling dates to the 1970s or earlier,[20] and has been common since the early 2000s.[12,13,21−27] However, even purpose-built "mobile labs" are rarely deployed for extended periods, and often depend on trained research staff as drivers.[25−28] As a result, few mobile monitoring data sets have sufficient repetition frequency or statistical power to precisely reveal consistent long-term spatial patterns over wide areas. We consider here an alternative approach, equipping professionally driven fleet vehicles with air quality instruments, repeatedly sampling every street of an urban area, and applying data reduction algorithms to distill stable long-term spatial patterns from time-resolved data. This approach has been implemented for public transportation vehicles along fixed routes, including trams in Karlsruhe and Zürich.[24,29] We report here on a 1 year pilot study in the San Francisco Bay Area using extensive route-free driving representative of a broad sample of city streets. In addition to testing the feasibility of this approach at scale, we explicitly aimed to "overdesign" our sampling scheme to enable quantitative characterization of trade-offs between sampling frequency and measurement precision/accuracy. (A similar oversampling approach has been tested on shorter cycling routes in the U.S. and Belgium).[15,30,31] We demonstrate that our measurement approach is capable of precisely (±10−20% of median) revealing urban pollution gradients at very fine ∼30 m scales, or 10^4−10^5× greater spatial resolution than with urban-ambient monitors. Our results corroborate current understandings and also provide new insights into the spatial variability of urban air pollution.

2. MATERIALS AND METHODS

In brief, we equipped two Google Street View (SV) mapping vehicles with an Aclima environmental intelligence fast-response pollution measurement and data integration platform (Aclima, Inc., San Francisco, CA). Using these vehicles, we repeatedly measured weekday daytime concentrations of black carbon particles (BC), NO, and NO_2 over 1 year for every road within diverse residential, commercial and industrial areas of Oakland, CA. BC, NO, and NO_2 are key health relevant pollutants whose sources include vehicular traffic, shipping, industrial combustion, cooking, and heating. The large resulting data set (3×10^6 1-Hz measurements within a 30 km^2 area; 24 000 total vehicle-km on 750 road-km) is unique among mobile monitoring studies in its very high coverage density and repeat-visit frequency (average of 31 days and 200 1-Hz measurements for each 30 m of road, SI Figure S2). Through data reduction and bootstrap resampling[32] algorithms, we compute median ± standard error (SE) annual daytime concentrations for ∼21 000 unique road segments. While instantaneous pollution levels vary rapidly in on-road environments, by repeatedly sampling each road and computing long-term medians, we obtained stable, precise (±10−20%) estimates of time-integrated pollution at fine 30 m spatial scales. Overall, these data reduction methods produce maps of systematic spatial variation in long-term air pollution that are robust to the stochastic temporal variability in the underlying 1-Hz data.

2.1. Measurement Platform. Two Google Street View (SV) vehicles were equipped with the Aclima Ei measurement and data acquisition platform. This platform provides data management, quality control, and visualization functions, facilitating extensive, routine measurements. In the present configuration, monitors employed were fast-response (1 Hz) laboratory-grade analyzers: BC was measured using a photoacoustic extinctiometer, NO was measured using chemiluminescence, and NO_2 was measured using cavity-attenuation phase-shift spectroscopy. The inlet system was designed to minimize self-sampling and particle sampling losses. Further details of the instrumentation design, routine calibrations, and QA/QC protocols/algorithms are provided as SI.

2.2. Study Area Description and Sampling Protocol. Sampling during the 1 year study duration emphasized three main areas within Oakland, CA: West Oakland (WO, ∼10 km^2), Downtown Oakland (DT, ∼5 km^2), and East Oakland (EO, ∼15 km^2). WO is bounded by major interstate highways (I-880, I-980, I-580), the fifth-largest U.S. container port, and associated rail and trucking facilities. Residential blocks are interspersed with industries in this lower-income neighborhood. DT has mixed residential and commercial mid- and high-rise buildings. EO is divided between industrial and mixed-income residential areas.

We undertook mobile monitoring on weekdays from May 28, 2015 to May 14, 2016. During routine operation, cars left garages in either Mountain View, CA or San Francisco, CA at around 9:00 AM local time and drove to Oakland, CA for ∼6−8 h of driving. Barring operational constraints (e.g., maintenance), two cars were operated simultaneously on each driving day.

Drivers were provided daily driving assignments consisting of polygons (∼1−5 km^2) in which the driver was tasked with driving every road at least once. Drivers were instructed to drive in the normal flow of traffic. Mean speeds were ∼25 km h^{-1} on surface streets and ∼88 km h^{-1} on highways. Routine sampling was conducted during all seasons. Vehicles were operated without regard to weather, except during 1−2 exceptional storms that precluded safe driving. The prevailing wind direction for the study area was from the west (∼85% of all study hours; median wind speed 4 m s^{-1}). A total of 2.7 M 1-Hz observations, or 800 h, on ∼16 000 unique 30 m road segments were collected in core WO+DT+EO domain. Additional monitoring incorporated interstate highways linking the study areas and car maintenance garages (∼300 k 1-Hz measurements on ∼4500 unique 30 m road segments). Further information about the study domain and operational considerations are provided as SI, including detailed maps (Figure S1−S2).

2.3. Data Reduction. We developed a series of data reduction algorithms to convert our data set of ∼3 million instantaneous observations into estimates of median annual weekday concentrations for individual 30-m road segments. First, we accounted for the possible biases of daily diurnal variation in urban-background concentrations by applying an hourly multi-

DOI: 10.1021/acs.est.7b00891
Environ. Sci. Technol. 2017, 51, 6999−7008

plicative adjustment factor to our 1-Hz mobile data based on ambient concentrations at a regulatory fixed-site monitor in WO.[15,23,30,33] This adjustment approach makes the implicit assumption that temporal patterns are spatially invariant. This common assumption is conceptually imperfect but may be acceptable for well-mixed daytime hours.[15,23,30,33] In any case, the temporal adjustment had only a minor (±10%) impact on the observed spatial patterns in long-term concentrations, likely because the numerous repeated measurements were already balanced in space and time.

Next, we employed a "snapping" procedure to assign each 1-Hz measurement to the nearest 30 m road segment on the basis of measured GPS coordinates, thereby allowing repeated measurements along the same road to be analyzed as a group.[15] We chose to use 30 m road segments for analysis after weighing considerations of spatial resolution (smaller segments show more spatial variability) and sample size (outliers and GPS errors have proportionally greater influence when data are "thinly sliced"). A virtue of this data reduction step is that it ensures that road segments with a high number of raw 1-Hz samples (e.g., owing to low average speeds) are not over-represented in our spatial analyses: regardless of the number of 1-Hz samples, a single point estimate of concentration is produced for each road segment. We restrict our analysis to include only the ∼21 000 road segments in our study domain with at least 10 unique days of measurement between 8 am and 6:59 pm local time between 28 May 2015 and 18 May 2016. The typical road segment contains ∼150−250 individual 1-Hz samples collected on ∼20−50 distinct days. The SI provides further details on the performance of our "snapping" and temporal adjustment algorithms (see Figures S4−S5).

For each of the ∼21 000 road segments, we computed distributional parameters of repeated 1-Hz observations. Similar to some recent mobile monitoring studies,[15,30] but unlike others,[28] we explicitly chose not to filter out "peak" 1-Hz concentration measurements resulting from encounters with other vehicles' exhaust plumes in assessing spatial patterns. The frequency with which plumes occur in space and time provides valuable information about the conditions that give rise to on-road concentrations.[30] We evaluated both the median and mean as metrics of central-tendency. In initial study design, we had two a priori concerns about the possible use of the mean as a reliable metric: First, that a small number of extreme outlier observations (true concentration "peaks" or rare spurious measurements) might bias our estimation of "typical" concentrations for each road segment, and second, that if we under-sampled the tails of a skewed concentration distribution, we might not obtain stable means. Also, for a log-normal or similarly skewed distribution, median is generally a more appropriate measure of central tendency than is mean. Accordingly, we chose to use median concentrations as our core estimate of central tendency for 30 m road segments, and evaluated means in sensitivity analyses.

We used a set of bootstrap resampling procedures to quantify the effect of sample-to-sample variability and sampling error on the precision of central-tendency 30 m concentration estimates. For each individual road segment, we computed the standardized error (SE) of the median and mean concentration. As a metric of precision, we consider normalized SE: the ratio of the standard error of the median (mean) concentration to the median (mean) concentration itself (SI Table S4). On average, the normalized SE of individual 30 m median (mean) concentrations was low: respectively 20% (21%), 16% (15%), and 9% (8%) for BC, NO, and NO_2. Road segment mean concentrations were well correlated with medians (mean > median owing to positive skew, $r^2 \sim 0.6-0.9$). In sum, for our sample size, central-tendency concentrations can be estimated with good precision and minimal sampling error from stochastic variability. For large groups of road segments (e.g., all residential streets), we estimate the precision of the central tendency to be within ≪1% of the normalized SE.

The SI provides further information on bootstrapping and precision calculations, comparisons between mean and median metrics, and summary tables of raw and reduced data (SI Tables S2−S3). The distributions of all ∼21 000 30 m-median road segment concentrations for NO, NO_2, and BC are positively skewed, but based on a Kolmogorov−Smirnov test do not conform to a single parametric distribution (SI Figure S6).

2.4. Stability Analysis: Monte Carlo Subsampling. We utilize a subsampling analysis to investigate whether a less intensive program of repeated monitoring can reproduce the long-term pollution patterns observed from the full data set.[15,30,31] A specific question of interest here is whether there is a point of "diminishing return," beyond which additional repeat driving provides relatively little added information.

We use Monte Carlo simulation to repeatedly subsample our full data set to systematically introduce fewer days of driving for analysis. Briefly, we randomly sample without replacement $1 \leq N \leq 50$ unique drive days at each location from our full data set. Within our core domain, the mean road segment has 31 days of sampling (10% trimmed range: 17−49 days). For each value of N, we performed 250 random draws to produce 250 subsampled "maps" of 30 m median concentrations. For road segments with fewer than N days of sampling, the "subsampling" effectively includes all observations collected over the duration of our campaign. Thus, the subsampled maps converge to the result of the full data set as N approaches the total number of unique driving days for the full measurement campaign. We compute three metrics to compare the performance of each subsampled concentration map to that of our full data set. First, as a metric of precision, we computed the r^2 between each subsampled map and the corresponding full data set of 30 m median concentrations. Second, as a metric of bias, we compute the normalized root-mean-square error (normalized RMSE, or equivalently, the coefficient of variation of the RMSE, CV-RMSE) as the square root of the mean of the squared difference between each subsampled 30 m median concentration and its corresponding median from the full data set. Third, as a metric of the temporal stability of subsampled spatial patterns, we computed the intraclass correlation (ICC) of each subsampled iteration, grouped by 30 m road segments. For this application, ICC values of 0.75−1 reflect large and systematic spatial differences, with low residual temporal variability at each location (see Section S1.5). We find that spatial variability dominates the total variability in our data set, with ICC values in the range of 0.8−0.95 for all pollutants (see SI Table S5), indicating that our observed long-term spatial patterns are robust to stochastic variability among individual 1-Hz samples.

2.5. Data Mining: Spatial Patterns. We conducted two "data mining" investigations to explore the determinants of the spatial patterns that are revealed by our mobile monitoring data, specifically (i) near-highway distance-decay relationships and (ii) the effect of local, transient sources on spatial patterns.

Distance-decay relationships for pollutant concentrations near major roadways have been documented in the literature,[8,34,35] relying predominantly on experiments along carefully selected near-highway upwind-downwind transects.[35] Here, we demon-

DOI: 10.1021/acs.est.7b00891
Environ. Sci. Technol. 2017, 51, 6999−7008

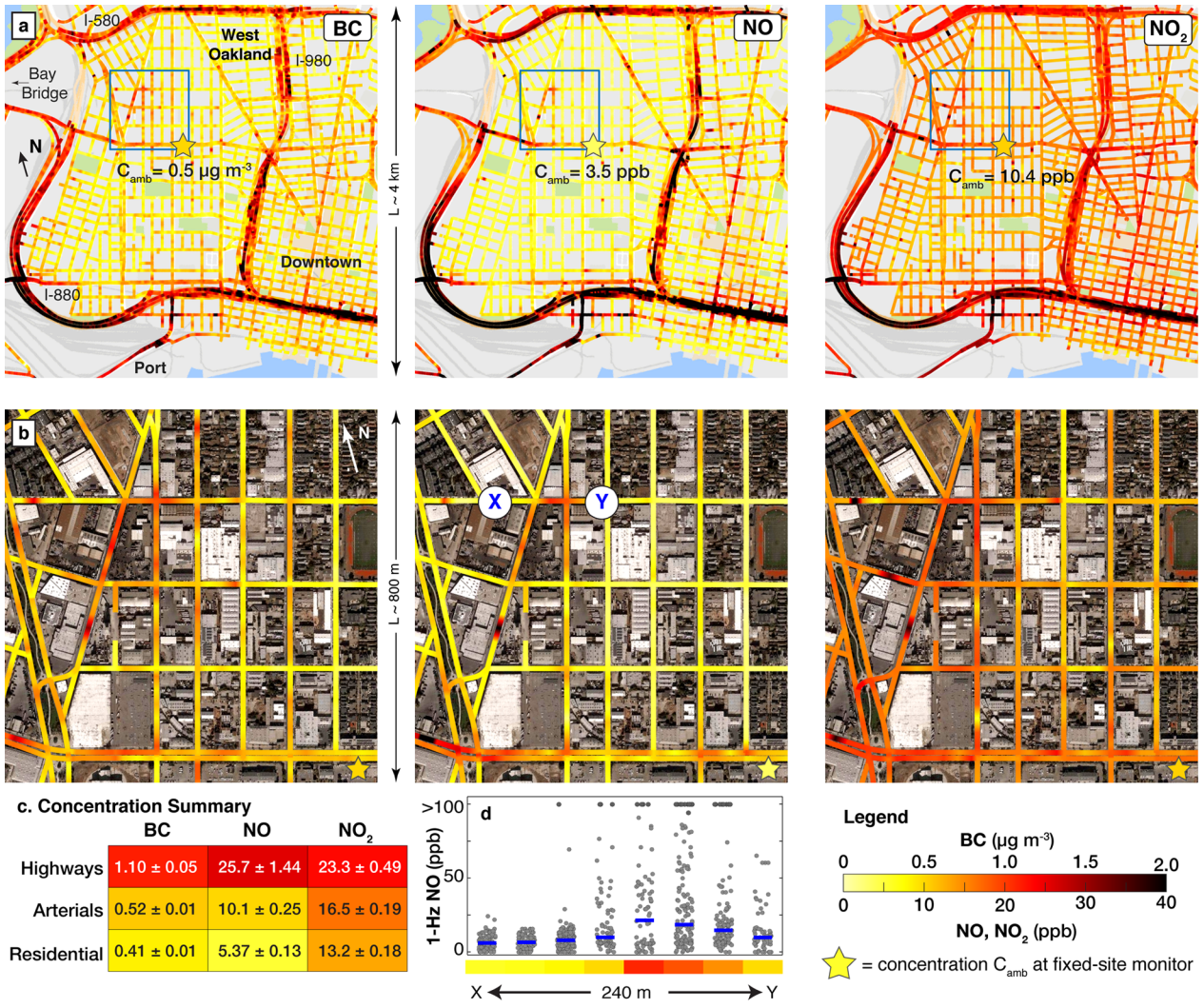

Figure 1. High-resolution mapping of time-integrated concentrations. Annual median daytime concentrations for 30 m-length road segments based on 1 year of repeated driving for a 16 km^2 domain in West Oakland [WO] and Downtown (a), and for a 0.6 km^2 industrial-residential area in WO (b). Median ± SE concentrations are tabulated by road type in c. Annual median daytime ambient concentrations C_{amb} at a regulatory fixed-site monitor in WO are plotted as shaded stars. Localized hotspots in b correspond to major intersections, industries, and businesses with truck traffic, and are interspersed with lower-income housing (see aerial image). Locations of hotspots are similar among pollutants. d, Distributions of 780 1-Hz NO measurements for a transect of eight 30 m road segments (see b, from point X to Y) to illustrate relationship between 1-Hz samples (~100 per segment over 1 year) and plotted long-term medians (colored bars, blue horizontal lines). Elevated levels near midpoint of transect are associated with operations at a metal recycler (see Figure 2). Wind rose data are provided in SI Figure S1, and show consistent westerly winds. Imagery © 2016 Google, map data © 2016 Google.

strate a "big data" approach that provides complementary information, using our full mobile data set to characterize time-averaged, isotropic (i.e., direction-independent) daytime distance-decay relationships. For every road segment within WO and DT, we computed a distance-to-nearest-highway parameter d ("spatial lag"). We bin all road segments by d, and compute the median concentration as a function of spatial lag using 50 m bins. For each pollutant we estimate a three-parameter exponential distance-decay relationship for the mean highway normalized concentration ratio as a function of spatial lag. The SI provides further detail on this fitting approach.

To investigate how localized or transient emissions sources contribute to the on-road concentrations measured by our mobile monitors, we employed a peak detection algorithm.[25,28,36,37] The basic conceptual approach uses a moving-window function to identify a localized concentration baseline, and then attributes the difference between the measured value and the baseline to short-duration concentration "peaks". We applied a 10 s moving average filter to the entire input data set to prevent spurious extreme low values in the raw data (e.g., instrument noise) from influencing the baseline determination. We established the concentration baseline for each second in this 10 s smoothed data set as the smaller of two quantities: the instantaneous value in the data set, or the p = fifth percentile concentration within a moving window of t = 120 s. By selecting the fifth percentile, the algorithm identifies a value that is representative of the cleanest local conditions, which are more influenced by the urban background than by localized sources. We chose t = 120 s to ensure that the time window was longer than the typical traffic light cycle, but short enough that the baseline concentrations on surface streets was established using measurements collected within ~1 km of each location (30 km/h for 2 min = 1 km).

DOI: 10.1021/acs.est.7b00891
Environ. Sci. Technol. 2017, 51, 6999−7008

b. Illustrative multi-pollutant hotspots

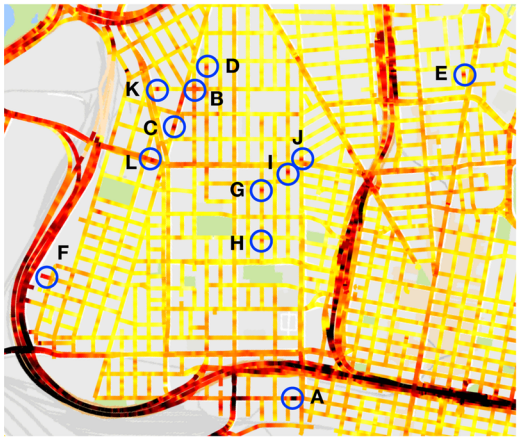

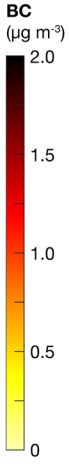

c. Description of identified hotspots

ID	BC	NO	NO_2	N_{days}	Plausible sources / hypotheses
A	+	~	+	38	Truck traffic and intersection
B	+	+	+	29	Metals recycling business
C	+	+	+	41	Cement plant and automotive shop
D	+	×	~	28	Warehouses with forklifts
E	+	~	+	23	Car dealer, vehicle "smog check"
F	+	×	~	17	Near recycling business; trucks; near I-880 frontage road
G	+	+	+	26	Towing lot, residential "hangout" area
H	+	+	+	24	Residential, no clear hypothesis
I	+	+	+	23	Warehouse and parking lot
J	+	~	+	40	Major intersection, parking lots, drive-through restaurant
K	+	+	+	24	Forklift dealership
L	+	+	+	52	Trucking, tire shops

Figure 2. Illustrative pollution hotspots. a. Street View and aerial imagery of the metals recycling cluster highlighted in Figure 4a–c. Frequent heavy-duty and medium-duty truck traffic is evident in repeated Street View images. b,c. Multipollutant hotspots (i.e., prominent local concentration outliers) were identified from BC, NO, and NO_2 median concentrations as described in SI. Twelve illustrative hotspots labeled A–L here, overlaid on the 30 m BC map in b for context. List in c enumerates possible emissions sources for each illustrative hotspot, with the following classification scheme for each pollutant: (+) indicates a prominent localized hotspot or cluster of roads where concentrations are sharply elevated above nearby background levels, (~) indicates a less prominent hotspot or cluster with moderately elevated levels, and (×) indicates the absence of a clearly discernible hotspot. Imagery © 2016 Google, map data © 2016 Google.

After establishing the baseline concentration, we derived the peak fraction parameter PF by computing (*i*) the mean baseline value over all repeated observations, and (ii) the mean 10s-smoothed observed concentration. Then, we compute PF as 1.0 minus the ratio of the mean baseline value to the mean observed concentration. Thus, PF is an indicator of the contribution to mean observed levels on each road segment of concentrations above the mean local baseline. While PF is inherently a semiquantitative indicator metric that is somewhat influenced by parameter choice, it usefully reveals spatial patterns in the density and magnitude of local, transient emissions sources. As a sensitivity analysis, we computed PF where the moving window period *t* was doubled to 4 min. For that analysis, overall spatial patterns in PF were nearly identical, but with an upward shift of 5–10% in PF: a longer window results in somewhat lower and more spatially homogeneous baseline concentrations.

3. RESULTS AND DISCUSSION

3.1. Spatial Patterns and Hotspots. Our mobile monitoring data set paints a vivid picture of within-urban pollution patterns, revealing remarkable and stable heterogeneity in daytime weekday pollutant concentrations (Figure 1, Figure S7). Figure 1b illustrates fine-scale variability in pollution for an indicative 0.6 km^2 industrial/residential zone in West Oakland (WO). Within this small area, time integrated 30-m median primary pollutant concentrations vary by >5× within individual

DOI: 10.1021/acs.est.7b00891
Environ. Sci. Technol. 2017, 51, 6999–7008

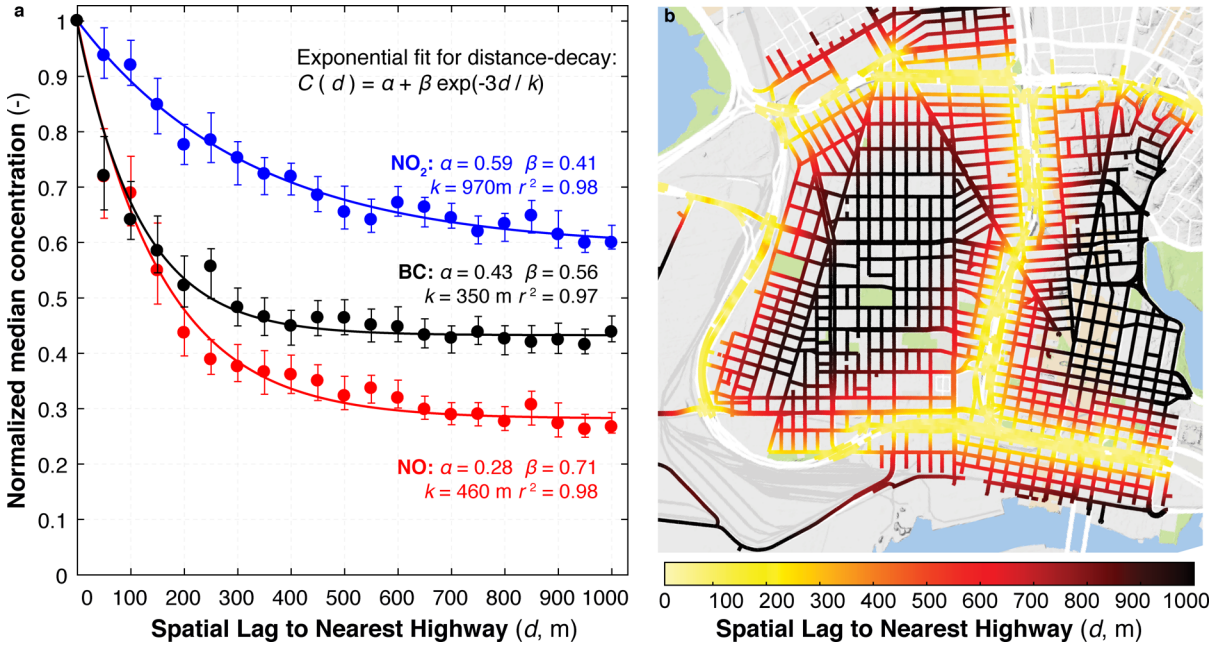

Figure 3. Decay of concentrations from major highways into city streets for WO and DT. a. Plotted points represent the ratio of median concentrations at a given distance from highways (d, "spatial lag") to median on-highway concentrations; error bars present standard error from bootstrap resampling. An unconstrained three parameter exponential model reproduces observed decay relationships with high fidelity. Here, the parameter α represents the ratio of urban-background to highway concentrations ($d \rightarrow \infty$), β represents the additional increment in pollution at near-highway conditions, and the decay parameter k governs the spatial scale of the decay process. The value of α is intermediate for BC (primary, conserved pollutant); lower for NO (consumed rapidly during daytime by reaction with O_3) and higher for NO_2 (elevated background from regional secondary photochemical conversion from NO). Data in SI demonstrate that parameter estimates are consistent among alternative fitting approaches. b. Distance-to-highway metric d for surface streets in WO and DT, computed based on the harmonic mean distance of each surface street segment to closest portion of the four major highways in the domain (see SI). Map data © 2016 Google.

city blocks, and by >8× overall, as the result of local emissions sources and traffic congestion. A surprising feature throughout our data set is the ubiquity of persistent daytime "hotspots" (length <100 m), tentatively classified as locations where concentrations of multiple pollutants exceed nearby ambient levels by 50% or more. Figure 2 presents data and plausible causes for an indicative set of hotspots based on analysis of Google Street View imagery. Examples include intersections along a major truck route, vehicle repair facilities, and industrial sites with associated truck traffic. As one indication of a localized source, most hotspots show sharp spatial "peaks" for multiple pollutants. (For the full data set, spatial patterns of 30 m-median concentrations for the three pollutants are moderately correlated, r^2: BC-NO = 0.71, NO-NO_2 = 0.57, BC-NO_2 = 0.50). The SI provides further detail on the hotspot identification scheme.

To demonstrate how hotspots consistently emerge from time-resolved data, Figure 1d shows long-term median and 1-Hz concentrations for the 240 m transect labeled X–Y in Figure 1b. Over the short length of this transect, time-integrated median NO levels rise and fall 4×. Concentrations are highest directly in front of the entrance to a metals recycling facility, where the 1-Hz distribution exhibits a large number of high NO concentrations. SV and aerial photos show a high volume of trucks and heavy equipment operating at this facility (Figure 2).

At broader spatial scales, pollutant levels differ substantially among three major road classes: highways, arterial roads, and residential streets (Figure 1). Median weekday daytime concentrations for WO and Downtown Oakland (DT) residential streets are approximately consistent with daytime observations at a regulatory fixed-site monitor in West Oakland (Figure 1c, road vs ambient: 0.41 ± 0.01 vs 0.50 $\mu g\ m^{-3}$ BC, 5.3 ± 0.11 vs 3.5 ppb NO, 13.2 ± 0.18 vs 10.4 ppb NO_2). In contrast, concentrations on busier streets and highways are substantially elevated above urban-background levels. For BC, median highway [arterial] concentrations exceed those on residential streets by a factor of 2.7 [1.3]; for NO by a factor of 4.8 [1.9]; and for NO_2 by a factor of 1.8 [1.3]. Atypically high pollutant concentrations for a given road class are evident in several areas of Figure 1, especially for NO and BC. Median concentrations on city-designated truck routes linking highways to industrial areas are 1.9–3.6× higher than on other surface streets (SI Table S6). We observe consistently higher BC and NO levels (1.5–2.0× higher) on I-880 (high truck density) than on I-580 (trucks prohibited, see SI and Figure S8).

3.2. Distance-Decay Relationships. Between the extremes of polluted freeways and cleaner residential streets, concentrations on average follow "distance-decay" relationships similar to those observed elsewhere.[8,9,34,35] An unconstrained three parameter exponential model, $C(d) = \alpha + \beta \exp(-3d/k)$, reproduces the concentration-distance relationship $C(d)$ with high fidelity ($r^2 \geq 0.96$, see Figure 3). Here, the isotropic parameter d reflects the distance to highways (m), the urban background parameter α represents concentrations far-from-highway ($d \rightarrow \infty$), the near-road parameter β represents the concentration increment resulting from proximity to the highway, and the decay parameter k governs the spatial scale over which concentrations relax to α. For all pollutants, estimated values of $(\alpha + \beta) \sim 1.0$, indicating that the combined contribution of the urban background and the near-highway increment approaches the levels observed on highways.

DOI: 10.1021/acs.est.7b00891
Environ. Sci. Technol. 2017, 51, 6999–7008

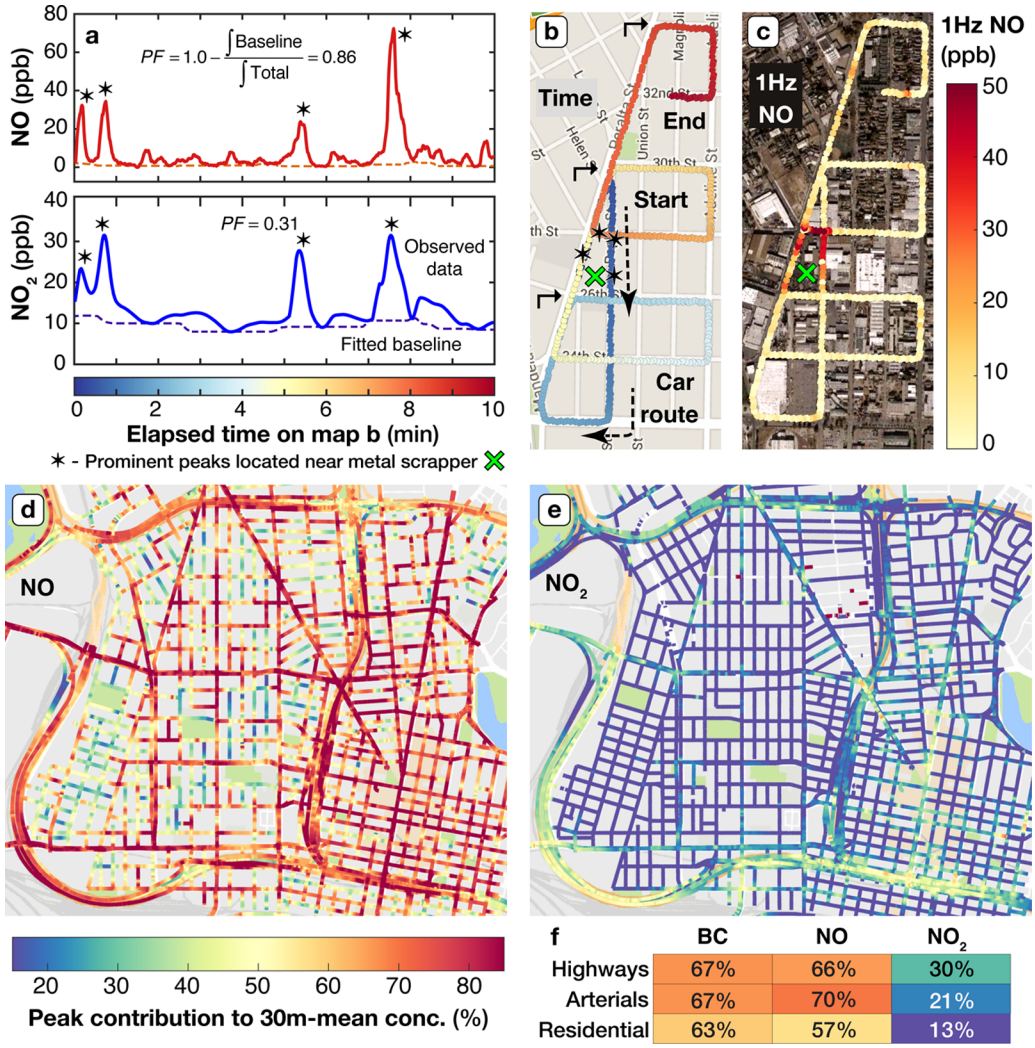

Figure 4. Identification of localized concentration peaks. a. Example 10 min time series of NO and NO_2 on afternoon of 4/22/2016. Baseline-fitting algorithm decomposes measurements (solid traces) into an ambient baseline component (dashed lines) and a high-frequency component indicative of localized pollutant sources ("peaks", difference between observation and baseline). Peak fraction PF indicates contribution of peaks to total sampled mass. PF is high for NO (low baseline, sharp peaks), and low for NO_2 (elevated ambient levels from photochemistry). Temporal progress along route indicated by blue-white-red color scale in a, and mapped in space in b. The drive route for these 10 min is a 4 km sequence of right-hand turns. As indicated by the time color scale in a and b, the starred NO peaks are spatially concentrated around a single city block with a scrap metal plant (marked × in b and c, cf. Figure 1b and Figure 2a). c, Spatial concentration profile for this example period. d,e,f. Application of peak-separation algorithm to entire data set. d,e. Blue-green-red color scale for PF quantifies fraction of mean concentration at each 30 m road segment attributable to transient peaks. f. Median PF values by road class. Imagery © 2016 Google, map data © 2016 Google.

Results in Figure 3 represent average weekday daytime decay patterns. These results reflect the average surface-street to highway concentration ratio as a function of d; as averages, they do not explore temporal differences (traffic, meteorology), the impact of wind direction, or heterogeneity among individual road segments. Interestingly, the fitted values of the parameters α and β correspond closely (within ±5%) to the results of the comprehensive meta-analysis of Karner et al. (2009).[8] Consistent with expectations about sources and atmospheric dynamics, our observed distance-decay relationships are sharpest for NO, intermediate for BC, and most shallow for NO_2. BC and NO are primary air pollutants from combustion sources. Unlike BC, NO is rapidly depleted during daylight hours by reaction with ozone ($NO + O_3 \rightarrow NO_2$, $\tau \sim 1-5$ min).[38] Because most (but not all[39,40]) daytime NO_2 is formed through secondary chemistry, spatial patterns of NO_2 tend to be more homogeneous than NO or BC. Further analysis of the robustness of our decay fitting approach and comparison with Karner et al. is provided as SI.

3.3. Localized Concentration Peaks. To further elucidate determinants of spatial patterns in air pollution, we mined the time-resolved data that underlie long-term median concentrations. The time evolution of concentrations collected by a mobile monitor reflects the superposition of (i) spatiotemporally localized concentration peaks from primary emissions and (ii) a comparatively less variable urban background condition.[28,37] Figure 4a illustrates the application of our baseline-and-peak decomposition algorithm to a 10 min excerpt from our WO mobile monitoring data. Four coincident NO and NO_2 peaks in this time series correspond in space (Figure 4b,c) to roads on the perimeter of the metals recycling facility illustrated in Figure 1b, demonstrating how spatially localized peaks are superimposed onto the urban background. For measurements at each 30 m road segment, we estimate the fractional contribution of localized

DOI: 10.1021/acs.est.7b00891
Environ. Sci. Technol. 2017, 51, 6999−7008

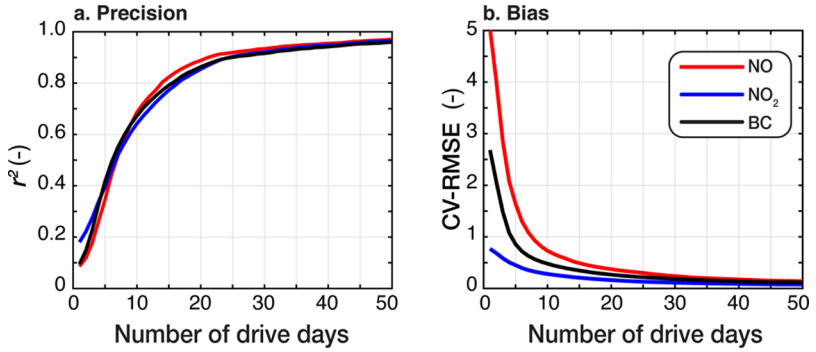

Figure 5. Scaling analysis through systematic subsampling. Using the systematic subsampling algorithm described in Section 2.4, we investigated the relationship between number of drive days and metrics of precision and bias. a. Mean subsampled r^2 as a function of 30 m-median road segment concentrations relative to the full data set, plotted as function the number of unique drive days for BC, NO, and NO_2. See SI for details of the subsampling algorithm and r^2 calculations. b. Mean subsampled coefficient of variation of root mean squared errors (CV-RMSE) versus the number of unique drive days for BC, NO, and NO_2.

sources to observed conditions ("peak fraction", PF) as 1.0 minus the ratio of the mean 30-m baseline concentration to mean 30-m observed concentration (Figure 4d–f). (Thus, at any given location, the observed 30 m median concentration is algebraically equivalent to the sum of the baseline plus peak contributions). Median values of PF are highest for NO and BC (~65%), indicating the predominant contribution of transient localized sources (e.g., traffic, industrial facilities). Spatial variations in PF values (Figure 4d) reveal that the urban background dominates NO levels on low-traffic residential streets (PF ~ 25–40%), whereas transient peaks govern concentrations on arterials (PF ~ 60–80%) and near industrial facilities. In contrast, for NO_2, PF is consistently low (~20%), reflecting the high baseline contribution from photochemistry. Future work could explore whether PF and other derived metrics (e.g., pollutant ratios) may be useful in representing the "freshness" of emissions to inform epidemiological analyses of multipollutant mixtures.

Taken in combination, our findings suggest that consistent spatial variability of air pollution exists at much finer scales than is generally detected using conventional measurements and predicted by models. Because hotspots are revealed through repeated measurement, this approach may be useful for evaluating the fine-scale performance of LUR and other models that use spatial surrogate data. We demonstrate that weekday, daytime primary pollutant levels persistently vary by a factor of 2–8× or more within neighborhoods and individual city blocks. For the median road segment, the absolute concentration difference from the single WO ambient regulatory monitor is 32% (BC), 61% (NO), and 35% (NO_2) during weekday daytime hours. Sparse monitoring networks may therefore provide an imprecise approximation and underestimate the true variability in heterogeneous population exposures.

The implications of these findings for population exposure and public health depend in part on the degree to which on-road concentrations can represent exposures. Many epidemiological studies use predicted home-address concentrations as a proxy for long-term personal exposures. These predicted home-address concentrations are often based upon models derived from roadside measurements given the ease of access to roadsides (e.g., utility poles) for monitoring. Recent research suggests that on-road concentrations can be well correlated with residential address exposures, even when on-road concentrations are higher than surrounding off-road areas owing to proximate traffic emissions.[17,41] Future work could validate the predictive power of *routine* mobile monitoring data using either residential fixed-site or personal exposure measurements.

3.4. Scaling and Future Prospects. Through systematic subsampling of our weekday daytime measurement data set, we find that 10–20 drive days (or 2–3× fewer data than collected here) are sufficient to reproduce key spatial patterns with good precision and low bias (Figure 5). The following trends hold: A small number of drive days ($N < 5$) typically results in a poor approximation of long-term spatial patterns from the full data set, with generally low precision (r^2) and high bias (CV-RMSE). However, each additional sampling day, across a year, results in a substantial improvement in r^2 and CV-RMSE. For our data set, diminishing returns for improvement in r^2 set in at ~10–20 drive days, with mean r^2 for BC and NO approaching 0.7 after 10 days of driving, and approaching 0.9 after 20–25 days of driving. Mean values of ICC (SI Figure S9) are generally high for 10 or fewer drive days, indicating that stochastic temporal variability from a small number of drive days does not obscure an overall spatially dominated pollution pattern. Similar conclusions on the number of sampling days required for convergence to stable patterns have recently been reported in studies using repeated bicycle-based BC and PM measurements.[15,30,31] Our sampling was restricted to weekday daytime conditions; in general, spatial patterns may differ at other times (nights, weekends, holidays).[42] Future work may reveal whether similar scaling considerations hold over a broader range of conditions, and in locales with less consistent meteorology than Oakland.

This study demonstrates a straightforward approach for dramatically increasing the spatial resolution with which air pollution is measured. The instrumentation costs of this technique using reference-grade monitors are perhaps comparable to those of traditional ambient monitoring. However, this routine mobile monitoring approach can provide several orders of magnitude more spatial information, albeit with lower temporal resolution. Future developments in fast-response low-cost sensor technologies could lower the costs of this approach. Moreover, in future studies, a considerably less intensive sampling scheme may provide similar results (Figure 5). Here, we employed Google SV vehicles to enable future analyses of contemporaneous 3D imagery, but other vehicle fleets (e.g., taxis, delivery vehicles, public transit) could routinely collect analogous data by repeatedly driving fixed or variable routes within a city. To facilitate scaling, our data reduction algorithms could be easily automated. Equipping ~500 such vehicles could enable high-resolution mapping of the 25 largest

DOI: 10.1021/acs.est.7b00891
Environ. Sci. Technol. 2017, 51, 6999–7008

U.S. urban areas, which in combination account for ~50% [36%] of the U.S. urban [total] population. Likewise, prior experience[12] suggests that this approach could be extended to global megacities (world's 20 largest cities have 480 M people, >10% of world urban population[43]) and to the thousands of other cities where air quality management is impaired by an absence of robust monitoring infrastructure. Future research could explore whether this approach can effectively be translated to such settings.

Routine availability of high-resolution air quality data in all major urban areas could have transformative implications for environmental management, air pollution science, epidemiology, public awareness, and policy. By highlighting localized pollution hotspots, these data may identify new opportunities for pollution control. Street-level air quality data can complement, challenge, and validate other diverse air quality data sets, including regulatory data, CTM outputs, land-use regression predictions, and remotely sensed observations. In turn, this refinement can help address exposure misclassification in epidemiological studies.[44,45] Through combination with personal GPS data on smartphone applications, rich "personal exposure analytics" become possible,[46,47] which could inform epidemiological studies and alter personal behavior, much as real-time traffic data now inform individual driving patterns. Broader societal consequences of the public awareness enabled by high-resolution pollution maps might include shifts in urban land-use decisions, regulatory actions, and in the political economy of environmental "riskscapes".

■ ASSOCIATED CONTENT

Supporting Information

The Supporting Information is available free of charge on the ACS Publications website at DOI: 10.1021/acs.est.7b00891.

Text, figures and tables with detailed information on experimental methods, QA/QC procedures, sampling protocols, data reduction/analysis techniques, supplemental analyses, and a data dictionary (PDF)

High-resolution concentration data (XLS)

■ AUTHOR INFORMATION

Corresponding Author

*E-mail: jsapte@utexas.edu.

ORCID

Joshua S. Apte: 0000-0002-2796-3478

Notes

The authors declare no competing financial interest.

■ ACKNOWLEDGMENTS

We gratefully acknowledge the contributions of K. Tuxen-Bettman, A. Raman, R. Moore, L. Vincent, C. Owens, D. Herzl, O. Puryear, A. Teste, M. Gordon, B. Beveridge, L. Clark, M. Chu Baird, C. Ely, A. Roy, J. Choi, R. Alvarez, S. Fruin, D. Holstius, P. Martien, and the Google Street View and Aclima mobile platform teams. Funding was provided by a grant from Signe Ostby and Scott Cook to Environmental Defense Fund. JSA was supported by a Google Earth Engine Research Award, MML is employed by Aclima, Inc., and TWK has been an investigator on unrelated research sponsored by Aclima. Data will be made available in an interactive online archive.

■ REFERENCES

(1) Apte, J. S.; Marshall, J. D.; Brauer, M.; Cohen, A. J. Addressing global mortality from ambient $PM_{2.5}$. *Environ. Sci. Technol.* **2015**, *49*, 8057−8066.

(2) Lim, S. S.; Vos, T.; Flaxman, A. D.; Danaei, G.; Shibuya, K.; Adair-Rohani, H.; Amann, M.; Anderson, H. R.; Andrews, K. G.; Aryee, M.; et al. A comparative risk assessment of burden of disease and injury attributable to 67 risk factors and risk factor clusters in 21 regions, 1990−2010: A systematic analysis for the Global Burden of Disease Study 2010. *Lancet* **2012**, *380*, 2224−2260.

(3) Pope, C. A.; Dockery, D. W. Health effects of fine particulate air pollution: Lines that connect. *J. Air Waste Manage. Assoc.* **2006**, *56*, 709−742.

(4) Brook, R. D.; Rajagopalan, S.; Pope, C. A., III; Brook, J. R.; Bhatnagar, A.; Diez-Roux, A. V.; Holguin, F.; Hong, Y.; Luepker, R. V.; Mittleman, M. A.; et al. Particulate matter air pollution and cardiovascular disease: An update to the scientific statement from the American Heart Association. *Circulation* **2010**, *121*, 2331−2378.

(5) Carvalho, H. The air we breathe: differentials in global air quality monitoring. *Lancet Respir. Med.* **2016**, *4*, 603−605.

(6) Brauer, M.; Freedman, G.; Frostad, J.; van Donkelaar, A.; Martin, R. V.; Dentener, F.; Dingenen, R. v.; Estep, K.; Amini, H.; Apte, J. S.; et al. Ambient air pollution exposure estimation for the Global Burden of Disease 2013. *Environ. Sci. Technol.* **2016**, *50*, 79−88.

(7) Zhang, K. M.; Wexler, A. S.; Zhu, Y. F.; Hinds, W. C.; Sioutas, C. Evolution of particle number distribution near roadways. Part II: the 'Road-to-Ambient' process. *Atmos. Environ.* **2004**, *38*, 6655−6665.

(8) Karner, A. A.; Eisinger, D. S.; Niemeier, D. A. Near-roadway air quality: Synthesizing the findings from real-world data. *Environ. Sci. Technol.* **2010**, *44*, 5334−5344.

(9) Zhu, Y. F.; Hinds, W. C.; Kim, S.; Shen, S.; Sioutas, C. Study of ultrafine particles near a major highway with heavy-duty diesel traffic. *Atmos. Environ.* **2002**, *36*, 4323−4335.

(10) Marshall, J. D.; Nethery, E.; Brauer, M. Within-urban variability in ambient air pollution: Comparison of estimation methods. *Atmos. Environ.* **2008**, *42*, 1359−1369.

(11) Morello-Frosch, R.; Pastor, M.; Sadd, J. Environmental justice and Southern California's "riskscape": the distribution of air toxics exposures and health risks among diverse communities. *Urban Affairs Review* **2001**, *36*, 551−578.

(12) Apte, J. S.; Kirchstetter, T. W.; Reich, A. H.; Deshpande, S. J.; Kaushik, G.; Chel, A.; Marshall, J. D.; Nazaroff, W. W. Concentrations of fine, ultrafine, and black carbon particles in auto-rickshaws in New Delhi, India. *Atmos. Environ.* **2011**, *45*, 4470−4480.

(13) Boogaard, H.; Kos, G. P. A.; Weijers, E. P.; Janssen, N. A. H.; Fischer, P. H.; van der Zee, S. C.; de Hartog, J. J.; Hoek, G. Contrast in air pollution components between major streets and background locations: Particulate matter mass, black carbon, elemental composition, nitrogen oxide and ultrafine particle number. *Atmos. Environ.* **2010**, *45*, 650−658.

(14) Jerrett, M.; Arain, A.; Kanaroglou, P.; Beckerman, B.; Potoglou, D.; Sahsuvaroglu, T.; Morrison, J.; Giovis, C. A review and evaluation of intraurban air pollution exposure models. *J. Exposure Anal. Environ. Epidemiol.* **2005**, *15*, 185−204.

(15) Hankey, S.; Marshall, J. D. Land use regression models of on-road particulate air pollution (particle number, black carbon, $PM_{2.5}$, particle size) using mobile monitoring. *Environ. Sci. Technol.* **2015**, *49*, 9194−9202.

(16) Reyes, J. M.; Serre, M. L. An LUR/BME framework to estimate $PM_{2.5}$ explained by on road mobile and stationary sources. *Environ. Sci. Technol.* **2014**, *48*, 1736−1744.

(17) Kerckhoffs, J.; Hoek, G.; Messier, K. P.; Brunekreef, B.; Meliefste, K.; Klompmaker, J. O.; Vermeulen, R. Comparison of ultrafine particle and black carbon concentration predictions from a mobile and short-term stationary land-use regression model. *Environ. Sci. Technol.* **2016**, *50*, 12894−12902.

(18) Snyder, E. G.; Watkins, T. H.; Solomon, P. A.; Thoma, E. D.; Williams, R. W.; Hagler, G. S. W.; Shelow, D.; Hindin, D. A.; Kilaru, V. J.;

Preuss, P. W. The changing paradigm of air pollution monitoring. *Environ. Sci. Technol.* **2013**, *47*, 11369−11377.
(19) West, J. J.; Cohen, A.; Dentener, F.; Brunekreef, B.; Zhu, T.; Armstrong, B.; Bell, M. L.; Brauer, M.; Carmichael, G.; Costa, D. L.; et al. What we breathe impacts our health: Improving understanding of the link between air pollution and health. *Environ. Sci. Technol.* **2016**, *50*, 4895−4904.
(20) Whitby, K. T.; Clark, W. E.; Marple, V. A.; Sverdrup, G. M.; Sem, G. J.; Willeke, K.; Liu, B. Y. H.; Pui, D. Y. H. Characterization of California aerosols–I. Size distributions of freeway aerosol. *Atmos. Environ.* **1975**, *9*, 463−482.
(21) Westerdahl, D.; Fruin, S.; Sax, T.; Fine, P. M.; Sioutas, C. Mobile platform measurements of ultrafine particles and associated pollutant concentrations on freeways and residential streets in Los Angeles. *Atmos. Environ.* **2005**, *39*, 3597−3610.
(22) Hudda, N.; Gould, T.; Hartin, K.; Larson, T. V.; Fruin, S. A. Emissions from an international airport increase particle number concentrations 4-fold at 10 km downwind. *Environ. Sci. Technol.* **2014**, *48*, 6628−6635.
(23) Larson, T.; Henderson, S. B.; Brauer, M. Mobile monitoring of particle light absorption coefficient in an urban area as a basis for land use regression. *Environ. Sci. Technol.* **2009**, *43*, 4672−4678.
(24) Hasenfratz, D.; Saukh, O.; Walser, C.; Hueglin, C.; Fierz, M.; Arn, T.; Beutel, J.; Thiele, L. Deriving high-resolution urban air pollution maps using mobile sensor nodes. *Pervasive and Mobile Computing* **2015**, *16* (Part B), 268−285.
(25) Bukowiecki, N.; Dommen, J.; Prevot, A. S. H.; Richter, R.; Weingartner, E.; Baltensperger, U. A mobile pollutant measurement laboratory-measuring gas phase and aerosol ambient concentrations with high spatial and temporal resolution. *Atmos. Environ.* **2002**, *36*, 5569−5579.
(26) Pirjola, L.; Parviainen, H.; Hussein, T.; Valli, A.; Hameri, K.; Aaalto, P.; Virtanen, A.; Keskinen, J.; Pakkanen, T. A.; Makela, T.; et al. "Sniffer" - a novel tool for chasing vehicles and measuring traffic pollutants. *Atmos. Environ.* **2004**, *38*, 3625−3635.
(27) Kolb, C.; Herndon, S. C.; McManus, J. B.; Shorter, J. H.; Zahniser, M. S.; Nelson, D. D.; Jayne, J. T.; Canagaratna, M. R.; Worsnop, D. R. Mobile laboratory with rapid response instruments for real-time measurement of urban and regional trace gas and particulate distributions and emissions source characteristics. *Environ. Sci. Technol.* **2004**, *38*, 5694−5703.
(28) Brantley, H. L.; Hagler, G. S. W.; Kimbrough, E. S.; Williams, R. W.; Mukerjee, S.; Neas, L. M. Mobile air monitoring data-processing strategies and effects on spatial air pollution trends. *Atmos. Meas. Tech.* **2014**, *7*, 2169−2183.
(29) Hagemann, R.; Corsmeier, U.; Kottmeier, C.; Rinke, R.; Wieser, A.; Vogel, B. Spatial variability of particle number concentrations and NOx in the Karlsruhe (Germany) area obtained with the mobile laboratory 'AERO-TRAM'. *Atmos. Environ.* **2014**, *94*, 341−352.
(30) Van den Bossche, J.; Peters, J.; Verwaeren, J.; Botteldooren, D.; Theunis, J.; De Baets, B. Mobile monitoring for mapping spatial variation in urban air quality: Development and validation of a methodology based on an extensive dataset. *Atmos. Environ.* **2015**, *105*, 148−161.
(31) Peters, J.; Theunis, J.; Van Poppel, M.; Berghmans, P. Monitoring PM_{10} and ultrafine particles in urban environments using mobile measurements. *Aerosol Air Qual. Res.* **2013**, *13*, 509−522.
(32) Efron, B. Bootstrap methods: another look at the jackknife. *Ann. Stat.* **1979**, *7*, 1−26.
(33) Dons, E.; Int Panis, L.; Van Poppel, M.; Theunis, J.; Wets, G. Personal exposure to black carbon in transport microenvironments. *Atmos. Environ.* **2012**, *55*, 392−398.
(34) Zhou, Y.; Levy, J. I. Factors influencing the spatial extent of mobile source air pollution impacts: a meta-analysis. *BMC Public Health* **2007**, *7*, 89.
(35) Zhu, Y.; Hinds, W. C.; Kim, S.; Sioutas, C. Concentration and size distribution of ultrafine particles near a major highway. *J. Air Waste Manage. Assoc.* **2002**, *52*, 1032−1042.
(36) Both, A. F.; Balakrishnan, A.; Joseph, B.; Marshall, J. D. Spatiotemporal aspects of real-time $PM_{2.5}$: Low- and middle-income neighborhoods in Bangalore, India. *Environ. Sci. Technol.* **2011**, *45*, 5629−5636.
(37) Watson, J. G.; Chow, J. C. Estimating middle-, neighborhood-, and urban-scale contributions to elemental carbon in Mexico City with a rapid response aethalometer. *J. Air Waste Manage. Assoc.* **2001**, *51*, 1522−1528.
(38) Seinfeld, J. H.; Pandis, S. N. *Atmospheric Chemistry and Physics: From Air Pollution to Climate Change*, 2nd ed.; Wiley-Interscience: Hoboken, NJ, 2006.
(39) Dallmann, T. R.; Harley, R. A.; Kirchstetter, T. W. Effects of diesel particle filter retrofits and accelerated fleet turnover on drayage truck emissions at the Port of Oakland. *Environ. Sci. Technol.* **2011**, *45*, 10773−10779.
(40) Jenkin, M. E. Analysis of sources and partitioning of oxidant in the UK—Part 2: contributions of nitrogen dioxide emissions and background ozone at a kerbside location in London. *Atmos. Environ.* **2004**, *38*, 5131−5138.
(41) Riley, E. A.; Schaal, L.; Sasakura, M.; Crampton, R.; Gould, T. R.; Hartin, K.; Sheppard, L.; Larson, T.; Simpson, C. D.; Yost, M. G. Correlations between short-term mobile monitoring and long-term passive sampler measurements of traffic-related air pollution. *Atmos. Environ.* **2016**, *132*, 229−239.
(42) Hu, S.; Fruin, S.; Kozawa, K.; Mara, S.; Paulson, S. E.; Winer, A. M. A wide area of air pollutant impact downwind of a freeway during pre-sunrise hours. *Atmos. Environ.* **2009**, *43*, 2541−2549.
(43) Brinkhoff, T. Major agglomerations of the world. http://citypopulation.de/world/Agglomerations.html 2016 (accessed February 14, 2017).
(44) Zeger, S. L.; Thomas, D.; Dominici, F.; Samet, J. M.; Schwartz, J.; Dockery, D.; Cohen, A. Exposure measurement error in time-series studies of air pollution: concepts and consequences. *Environ. Health Persp.* **2000**, *108*, 419−426.
(45) Sheppard, L.; Burnett, R. T.; Szpiro, A. A.; Kim, S.-Y.; Jerrett, M.; Pope, C. A.; Brunekreef, B. Confounding and exposure measurement error in air pollution epidemiology. *Air Qual., Atmos. Health* **2012**, *5*, 203−216.
(46) de Nazelle, A.; Seto, E.; Donaire-Gonzalez, D.; Mendez, M.; Matamala, J.; Nieuwenhuijsen, M. J.; Jerrett, M. Improving estimates of air pollution exposure through ubiquitous sensing technologies. *Environ. Pollut.* **2013**, *176*, 92−99.
(47) Nyhan, M.; Grauwin, S.; Britter, R.; Misstear, B.; McNabola, A.; Laden, F.; Barrett, S. R. H.; Ratti, C. "Exposure Track"—the impact of mobile-device-based mobility patterns on quantifying population exposure to air pollution. *Environ. Sci. Technol.* **2016**, *50*, 9671−9681.

DOI: 10.1021/acs.est.7b00891
Environ. Sci. Technol. 2017, 51, 6999−7008